Destruction and reinstatement of coastal hypoxia in the South China Sea off the Pearl River Estuary

Yangyang Zhao[1,2], Khanittha Uthaipan[1], Zhongming Lu[3], Yan Li[1], Jing Liu[1,4], Hongbin Liu[5,6], Jianping Gan[3,6,7], Feifei Meng[1], Minhan Dai[1]

[1]State Key Laboratory of Marine Environmental Science, Xiamen University, Xiamen, 361102, China
[2]Environmental Physics, Institute of Biogeochemistry and Pollutant Dynamics, ETH Zurich, Zurich, 8092, Switzerland
[3]Division of Environment and Sustainability, Hong Kong University of Science and Technology, Kowloon, Hong Kong SAR, China
[4]Marine Biogeochemistry Division, GEOMAR Helmholtz Centre for Ocean Research Kiel, Wischhofstraße 1–3, Kiel, 24148, Germany
[5]Division of Life Science, Hong Kong University of Science and Technology, Kowloon, Hong Kong SAR, China
[6]Department of Ocean Science, Hong Kong University of Science and Technology, Kowloon, Hong Kong SAR, China
[7]Department of Mathematics, Hong Kong University of Science and Technology, Kowloon, Hong Kong SAR, China

Correspondence to: Minhan Dai (mdai@xmu.edu.cn)

Abstract. We examined the evolution of intermittent hypoxia off the Pearl River Estuary during three cruise legs conducted in July 2018: one during severe hypoxic conditions before the passage of a typhoon and two post-typhoon legs showing destruction of the hypoxia and its reinstatement. The lowest ever regional dissolved oxygen (DO) concentration of 3.5 µmol kg^{-1} (~ 0.1 mg L^{-1}) was observed in bottom waters during Leg 1, with a ~ 660 km^2 area experiencing hypoxic conditions (DO < 63 µmol kg^{-1}). Hypoxia was completely destroyed by the typhoon passage but was quickly restored ~ 6 days later, resulting primarily from high biochemical oxygen consumption in bottom waters that averaged -14.6±4.8 µmol O$_2$ kg^{-1} d^{-1}. The shoreward intrusion of subsurface shelf waters contributed to an additional 8.6±1.7 % of oxygen loss during the reinstatement of hypoxia. Freshwater input-induced stratification, suppressing turbulent mixing induced by wind stress and/or tidal forcing, stabilized the water column and facilitated the hypoxia formation. The rapid reinstatement of summer hypoxia has a comparable timescale with water residence time and that of its initial disturbance from frequent tropical cyclones or high-wind events throughout the season. This has important implications towards better understanding the intermittent nature of hypoxia, and predicting coastal hypoxia in a changing climate.

1 Introduction

Coastal hypoxia has been increasingly exacerbated near the mouths of large rivers as a consequence of anthropogenic nutrient inputs (Gilbert et al. 2010, Rabalais et al. 2014, Breitburg et al. 2018). The rise in the size, intensity and frequency of eutrophication-induced hypoxia exposes coastal oceans to a higher risk of elevated N$_2$O and CH$_4$ production, enhanced ocean acidification and associated reductions in biodiversity, shifts in community structures and negative impacts on food security and livelihoods (Diaz and Rosenberg 2008, Vaquer-Sunyer and Duarte 2008, Naqvi et al. 2010).

Coastal hypoxia can be intermittent due to the dynamic nature of estuarine and coastal environments, where winds, tides, river

35   discharge and circulation patterns strongly affect the ventilation of oxygen-deficient waters (Wang and Justić 2009, Lu et al. 2018, Zhang et al. 2019). Constraints on oxygen supply can be easily eroded by changes in physical forcings, leading to the temporal alleviation of hypoxia (Laurent and Fennel 2019). Despite the wide application of oxygen budget analysis and modelling to diagnose the dominant processes driving the formation and maintenance of hypoxia (Yu et al. 2015, Li et al. 2016, Lu et al. 2018), the evolution of intermittent hypoxia, such as the destruction and reinstatement of hypoxia from

40   disturbance by tropical cyclones, remains to be better characterized (Testa et al. 2017). Specifically, the identification of key processes and timescale constraints for these hypoxia destruction and recovery processes is of critical importance in order to predict site-specific hypoxia and its cascading effects, and to forecast the long-term impact of hypoxia under a changing climate with higher-intensity extreme events (Knutson et al. 2010, Mendelsohn et al. 2012).

45   Large riverine nutrient loadings and the resulting eutrophication have recently tipped the lower Pearl River Estuary (PRE) and adjacent shelf areas into seasonally hypoxic systems (Yin et al. 2004, Rabouille et al. 2008, Su et al. 2017, Qian et al. 2018, Cui et al. 2019, Zhao et al. 2020). Modelling results have shown that summer hypoxia off the PRE is largely intermittent owing to high-frequency variations in wind forcing and tidal fluctuations (Wang et al. 2017, Huang et al. 2019). Hypoxia is often interrupted by the passage of typhoon, but redevelops quickly with a tendency toward rapid oxygen declines(Su et al. 2017,

50   Huang et al. 2019). The prevailing southwest monsoon usually favors the expansion of a quasi-steady-state freshwater bulge outside the entrance of the PRE (Gan et al. 2009, Lu et al. 2018) that promotes water column stability. However, it remains unclear how the interaction between wind stress and freshwater buoyancy affects the bottom oxygen conditions when the winds shift in the downwelling-favorable easterly or southeasterly direction, especially in the wake of tropical cyclones. Aerobic respiration of organic matter is largely responsible for the oxygen depletion here (Su et al. 2017, Qian et al. 2018).

55   Considering the oxygen consumption rate (OCR) has primarily been estimated based on incubations examining bacterial or community respiration (Su et al. 2017, Cui et al. 2019, Li et al. 2019), the actual magnitude of OCR during the hypoxia formation process has rarely been reported at large-scales. The role of lateral advection (or upwelling) also remains uncertain (Zhang and Li 2010, Lu et al. 2018, Qian et al. 2018, Cui et al. 2019).

60   The destruction and reinstatement of summer hypoxia off the PRE were investigated to examine the effects of freshwater inputs, winds and tides on water column stability and the formation and maintenance of hypoxia. With the aid of a three-endmember mixing model, the OCR and upwelling-induced reduction in initial oxygen levels were estimated to partition oxygen sinks for hypoxia regeneration after its destruction by a typhoon. The impacts of tropical cyclones on the evolution of seasonal hypoxia in river-dominated ocean margins is further discussed.

2 Materials and methods

2.1 Study area and cruise background

The shelf of northern South China Sea receives an average annual freshwater discharge of ~10,000 m^3 s^{-1} originating from the Pearl River, the 17th largest river in the world (Cai et al. 2004, Dai et al. 2014). Nearly four fifths of freshwater discharge occurs during the wet season, typically from April to September (Dai et al. 2014). The riverine freshwater extends offshore to form widespread plume over the shelf in summer (Gan et al. 2009, Cao et al. 2011, Chen et al. 2017), via eight outlets through three sub-estuaries (i.e., Lingdingyang, Modaomen and Huangmaohai; Fig. 1b). On the inner shelf, coastal upwelling interacts with the buoyant plume, propelled by the prevailing southwest monsoon and intensified along the eastward widened shelf (Gan et al. 2009, Chen et al. 2017). Nearly 7 tropical cyclones per year reached the NSCS from 1949-2019, half of which featured maximum wind speeds greater than 32.7 m s^{-1}.

Field observations and sampling were conducted onboard the R/V Haike 68 off the PRE on the inner-shelf of the northern South China Sea (NSCS) in the summer of 2018. The cruise was interrupted by the passage of typhoon SONTINH across the NSCS, ~ 350 km south of the PRE (Fig. 1a). Leg 1 (July 8-14) was the cruise period before the typhoon, and Leg 2 (July 21-25) and Leg 3 (July 26-29) were conducted after its passage (Fig. 1b). During each leg we collected samples from west to east and along the cross-shelf transects within isobaths of 10-35 m. Almost all stations in Leg 1 were revisited during Leg 2, and nearly half again during Leg 3. Eight stations were additionally revisited along the return voyage on July 31. Time-series observations with a sampling interval of 1 h were conducted at Station F303 for 26 h before Leg 2, beginning at 16:00 pm on July 19. In contrast to the typical southwesterly winds in the NSCS with average monthly wind speeds of < 6 m s^{-1} during June and September (Su 2004), easterly winds prevailed during the cruise period due to the typhoon, with the wind speeds increasing up to ~ 13 m s^{-1} (Fig. 1c) at the Waglan Island to the east of the study area (Fig. 1b).

2.2 Sampling and analysis

Temperature and salinity were determined using a SBE 917 plus conductivity-temperature-depth recorder (SeaBird Electronics, Inc.). Discrete samples were collected using 5 L free-flow water samplers mounted onto a Rosette sampling assembly. Dissolved oxygen (DO), dissolved inorganic carbon (DIC), total alkalinity (TA) and Chlorophyll *a* (Chl *a*) concentrations were measured at all stations with depth profiles from 1 m below the surface down to ~ 4-5 m above the bottom, generally at three depth layers. Additional high-resolution vertical samplings were conducted at 7-8 depth layers (Fig. 1b).

Salinity was calibrated against discrete water samples measured by a Multi 340i salimeter (WTW). The DO concentrations were measured onboard within ~ 12 h using the spectrophotometric Winkler method (Labasque et al. 2004), with a precision better than ±2 μmol L^{-1}. DIC was measured on ~ 0.5 mL acidified water samples using an infrared CO_2 detector (Apollo ASC-3) with a precision of ±2 μmol L^{-1} (Cai et al. 2004). TA was determined on 25 mL samples in an open-cell setting based on

the Gran titration technique (see details in Cai et al.(2010)) with a Kloehn digital syringe pump. The analytical precision was ±2 µmol L⁻¹. Both DIC and TA concentrations were calibrated against certified reference materials provided by Dr. A. G. Dickson at the Scripps Institution of Oceanography, University of California, San Diego. Chl *a* concentrations were determined

100   using a Trilogy laboratory fluorometer (Turner Designs, Inc.) following the standard fluorometric method (Welschmeyer 1994) and calibrated using a Sigma Chl *a* standard.
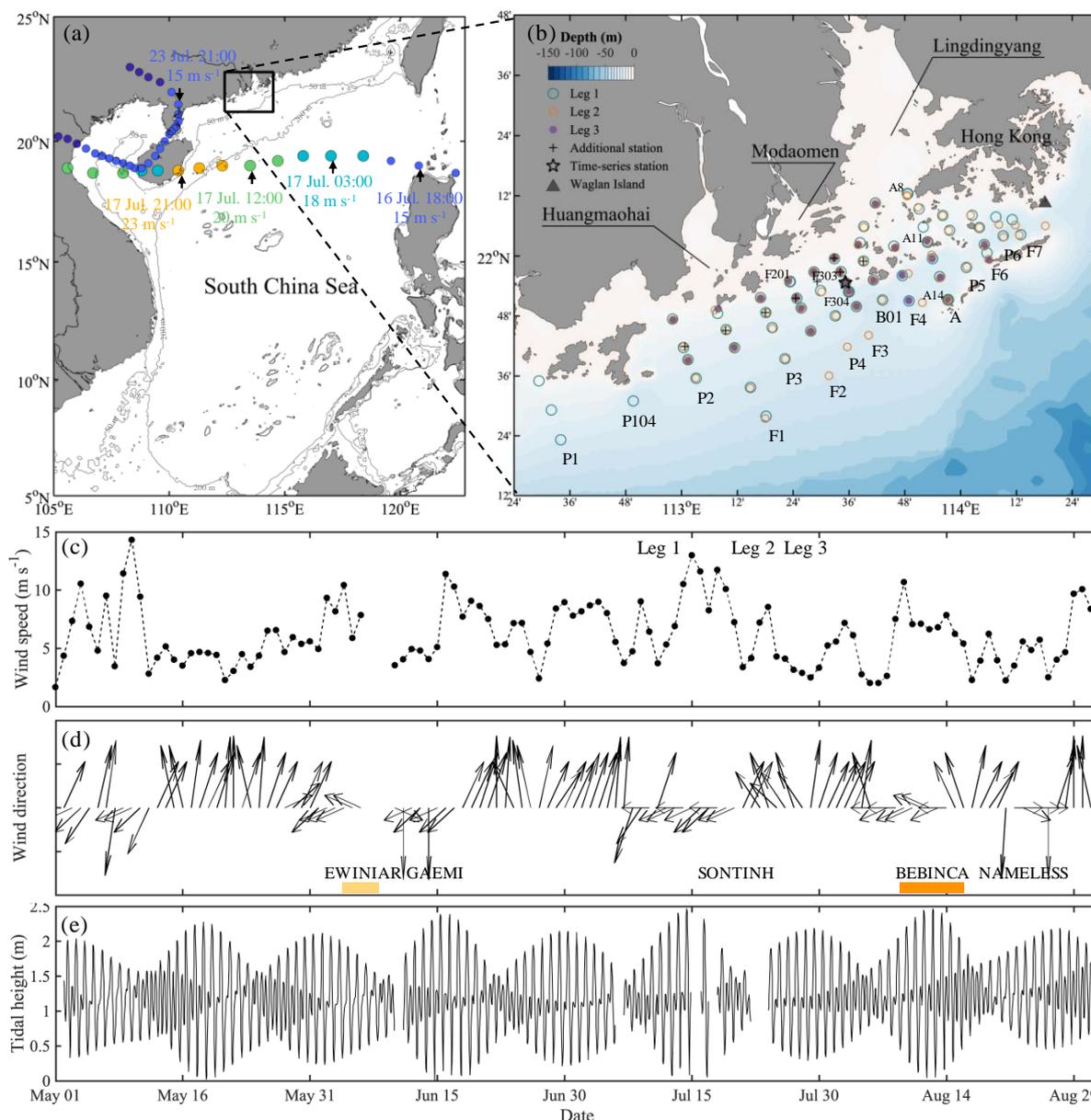

Figure 1: (a) Map of the study area on the northern South China Sea (NSCS) Shelf, showing the track of Typhoon SONTIHN (circles) across the NSCS during July 16-24, 2018. The color of the circles represents the magnitude of wind speed. Additionally, the smaller circles

Biogeosciences
Discussions

105 denote tropical depression (wind speeds ≤ 17.1 m s^{-1}) and the larger circles denote tropical storm (wind speeds within 17.2-32.6 m s^{-1}). The arrows denote the locations of the typhoon as marked with time and wind speed. The grey lines are the depth contours at 50 and 200 m. (b) Sampling stations on the NSCS shelf off the Pearl River Estuary in summer 2018. Time-series observations were conducted at Station F303 as marked by the star, and vertically high-resolution samplings were conducted at stations marked with bold circles. (c) The wind speed and (d) wind direction at Waglan Island (triangle in (b)) from May to August, 2018. Bars at the bottom of (d) mark times when tropical cyclones

110 impacted the NSCS. (e) The tidal height at the Dawanshan gauge station near Station F303 from May to August, 2018. The shaded area indicates the cruise periods for Leg 1 (grey), Leg 2 (pink) and Leg 3 (blue), respectively.

2.3 Oxygen consumption rate

From the perspective of Euler observations and based on mass balance, the DO changes (ΔDO) in bottom waters over a specified time interval at a specific site can be decomposed into components driven by physical mixing (ΔDO^{mix}) or

115 biochemical processes (ΔDO^{bc}). Here, we define the biochemical-induced DO decline with time (ΔDO^{bc}/Δt) as the oxygen consumption rate (OCR), and a positive OCR indicates the growth rate in DO levels due to biochemical processes. For revisited stations, ΔDO is the difference in DO values measured between the two sampling periods. The physical-mixing-induced DO variations were derived using a three-endmember mixing model, which construct the conservative mixing scheme among different water masses: Brackish Plume Water (PW), Offshore Surface Water (SW) and Upwelled Subsurface Water (SUB)

120 (Su et al. 2017, Cui et al. 2019, Zhao et al. 2020). The model is constrained by salinity (S) and potential temperature (θ) according to the following equations:

$$f_{PW} + f_{SW} + f_{SUB} = 1 \tag{1}$$

$$S_{PW} \times f_{PW} + S_{SW} \times f_{SW} + S_{SUB} \times f_{SUB} = S^{meas} \tag{2}$$

$$\theta_{PW} \times f_{PW} + \theta_{SW} \times f_{SW} + \theta_{SUB} \times f_{SUB} = \theta^{meas} \tag{3}$$

125 where the superscript 'meas' denotes measured values, and *f* represents the fraction that each endmember contributes to the *in situ* samples. Assuming that DO concentrations in surface waters were equilibrated with the atmosphere and the subsurface waters were isolated from the atmosphere due to restriction by stratification, these fractions were applied to predict conservative concentrations of DO (DO^{mix}) resulting solely from conservative mixing.

$$DO^{mix} = DO_{PW} \times f_{PW} + DO_{SW} \times f_{SW} + DO_{SUB} \times f_{SUB} \tag{4}$$

130

Similarly, ΔDO^{mix} is the difference in "conservative" DO values between visits, assuming that the advection of biochemically oxygen-consumed water masses is negligible in quasi-static bottom waters within the water residence time. As a result,

$$OCR = \Delta DO^{bc}/\Delta t = (\Delta DO - \Delta DO^{mix})/\Delta t \tag{5}$$

where Δt is the duration between the two observations. The uncertainty in the calculation of OCR mainly derives from the

135 estimation of conservative values predicted from the three-endmember mixing model. Sources of the composite uncertainty (ε) in derivation of DO^{mix} are associated with potential temperature (θ), salinity (S) and the dissolved oxygen (DO) values of endmembers.

$$\varepsilon_{DO^{mix}} = \sqrt{\sum_i^n \left[\left(f_i \cdot \sigma_{DO_i} \right)^2 + \left(DO_i \cdot \sigma_{f_i} \right)^2 \right]} \qquad (6)$$

where σ_{DO} and σ_f are uncertainties in the DO concentration and the fraction of each endmember i (i.e., PW, SW and SUB), the

140   latter of which can be calculated as

$$\sigma_{f_i} = \sqrt{\sum_j^n \left[\left(\partial f_i / \partial \theta_j \cdot \sigma_{\theta_j} \right)^2 + \left(\partial f_i / \partial S_j \cdot \sigma_{S_j} \right)^2 \right]} \qquad (7)$$

where j also denotes each endmember.

3 Results

3.1 Extensive hypoxia before the typhoon

145   A prominent two-layer structure was observed in the inner NSCS shelf off the PRE (Fig. 2a-h). In the surface layer, the
freshwater plume was attached to the coast when veering to the west as constrained by estuarine topography, the Coriolis force
(Wong et al. 2003), and easterly winds during Leg 1 (Fig. 1d), despite a freshwater bulge that remained near the mouth of the
Lingdingyang sub-estuary due to persistent southwesterly winds before the cruise (Fig. 1d) and the weak shelf current there
(Gan et al. 2009, Lu et al. 2018). A strong bloom occurred in the surface plume waters near the Huangmaohai sub-estuary,

150   characterized by high Chl a concentrations of > 20 μg L^{-1} and oversaturated DO of > 300 μmol kg^{-1} (equivalent to a DO
saturation level > 150 %) (Fig. 2c, d). The freshwater bulge also featured a relatively weak bloom, with Chl a concentrations
of ~ 10 μg L^{-1} and DO of ~ 250 μmol kg^{-1} (equivalent to a DO saturation level of ~ 125 %), likely owing to the high nutrient
concentrations, a favorable residence time and an abundance of photosynthetically active radiation (Lu and Gan 2015).

155   In the bottom layer, low-temperature, high-salinity shelf benthic waters intruded onshore to the 10-20 m isobaths below the
surface plume (Fig. 2e, f). An extensive hypoxic zone developed beneath the freshwater bulge and extended westwards along
the 20-30 m isobaths to the region off the Modaomen sub-estuary (Fig. 2g). To the east, a relatively weak hypoxic center
occurred adjoining the Hong Kong waters. Additionally, a smaller-scale hypoxic zone appeared under the surface bloom near
the Huangmaohai sub-estuary, a region which was not fully covered by survey measurements. The general pattern of hypoxic

160   zones was similar to that found in summer 2017 (Zhao et al. 2020), yet with a slight offshore shift. The minimum oxygen level,
3.5 μmol kg^{-1} (~ 0.1 mg L^{-1}), was observed in the bottom layer at Station F303, lower than the previously reported minimum
(~ 7 μmol kg^{-1} at Station F304 (Su et al. 2017)). Within the surveyed region, the total area of the hypoxic zone reached ~ 660
km^2 and the oxygen-deficit zone occupied ~ 1470 km^2. These findings indicate that summer hypoxia off the PRE has been
increasingly exacerbated in recent years (Su et al. 2017, Qian et al. 2018, Zhao et al. 2020).
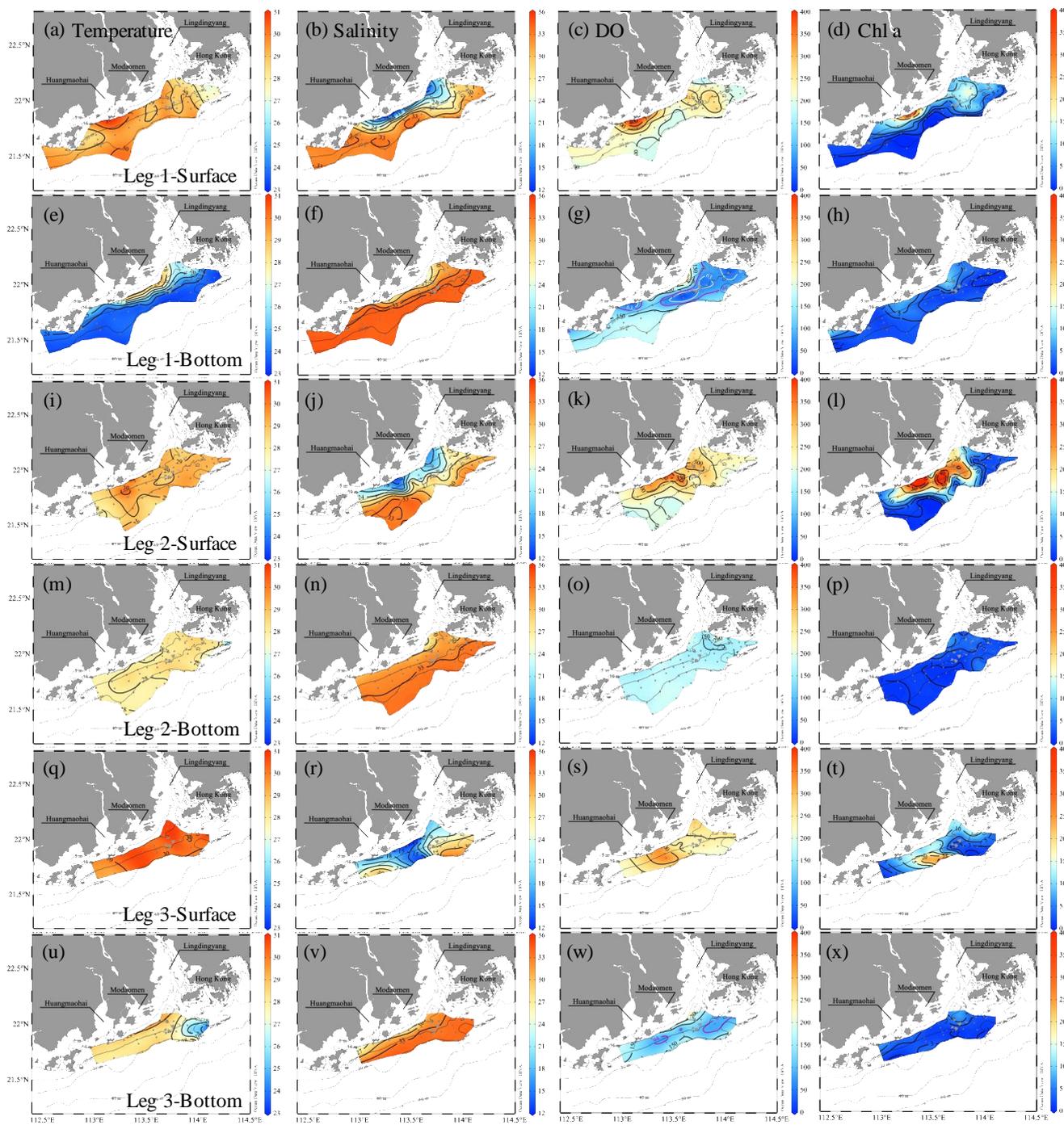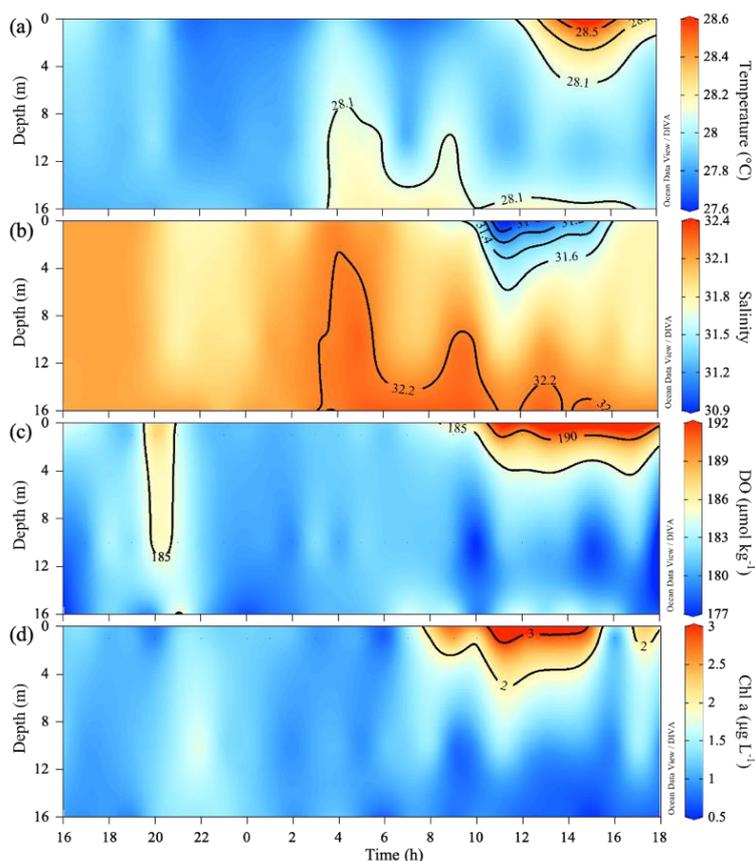
Figure 2: Distribution of temperature (°C), salinity, DO (μmol kg⁻¹) and Chl *a* concentrations (μg L⁻¹) at the surface and bottom water layers off the PRE during Leg 1 pre-typhoon, and during Legs 2 and 3 post-typhoon. The white and magenta contours in (g) and (w) show the hypoxic (DO < 63 μmol kg⁻¹) and oxygen-deficit (DO < 94 μmol kg⁻¹) zones.

Biogeosciences
Discussions
EGU
Open Access

3.2 Destruction of hypoxia by the typhoon

170   The spatial patterns of temperature, salinity, DO and Chl *a* concentrations all changed drastically from disturbance by intensified easterly winds during the typhoon period (Fig. 2i-p and Fig. 3). Time-series observations showed that the water column was vertically well mixed, as reflected by homogeneous distributions of temperature (~ 28 ℃) and salinity (~ 32), and greatly elevated DO levels (~ 180 µmol kg^{-1}) (Fig. 3a-c). The two-layer structure of the water column was then gradually restored, as observed during Leg 2 (Fig. 2i-p), with subdued winds that shifted to southwesterly in the following two days (Fig.

175   1c, d) and offshore spreading of the river plume. A stronger bloom was identified in the surface plume, widely spreading from the mouth of the Lingdingyang sub-estuary to near the Huangmaohai sub-estuary, potentially fueled by nutrients mixed upward from the deep in addition to riverine inputs (Wang et al. 2017, Qiu et al. 2019). The maximum Chl *a* concentration was > 40 µg L^{-1} off the Modaomen sub-estuary, accompanied by an extraordinarily high DO concentration of > 350 µmol kg^{-1} (Fig. 2k, l).

180

Figure 3: Time-series distribution of (a) temperature (°C), (b) salinity, (c) DO (µmol kg^{-1}) and (d) Chl *a* concentrations (µg L^{-1}) at Station F303 (see Fig. 1b) from July 19-20, 2018, post typhoon passage, showing the complete destruction and the subsequent rapid development of stratification.

In the bottom layer, however, hypoxia had been completely destroyed due to strong reaeration in the wake of the typhoon
185   travelling across the NSCS, replaced by a homogenous spatial distribution of relatively high DO concentrations (~ 171±16
µmol kg^{-1}) (Fig. 2o). The cross-shore gradients in temperature and salinity were also largely relaxed, with isotropically elevated
temperatures up to ~ 28 ℃ (Fig. 2m, n). The mid-depth distributions of temperature, salinity and DO concentrations showed
similar patterns as in the bottom layer (Fig. S1). Although the water column remained well-mixed under the surface layer,
freshwater buoyancy and weakened winds facilitated the revitalization of density stratification and subsequent oxygen decline
190   below the pycnocline. Indeed, the bottom water DO concentration at Station F303 decreased by ~ 18 µmol kg^{-1} compared to
that in the time-series observations and was lower than that at adjacent stations by ~ 9-22 µmol kg^{-1} when revisited during Leg
2 on July 22.

3.3 Reinstatement of hypoxia after the typhoon

With the dying-out of the typhoon after its landfall to the west of the study area on July 23 (Fig. 1a), the wind speed decreased
195   to < 5 m s^{-1} on July 25 while the wind direction remained from the southeast before it shifted to southwesterly on July 29 (Fig.
1c, d). The oxygen concentrations in bottom waters were noticeably lower (139-164 µmol kg^{-1} shallower than 20-m isobaths)
starting around July 23 during the second half of Leg 2 (Fig. 1b and 2o). During Leg 3, from July 26-29, hypoxia was present
again in the bottom layer, due to favorable conditions for its formation (Fig. 2q-x). The surface layer warmed to over 30 ℃,
strengthening the vertical stratification (Allahdadi and Li 2017). Inhibited by easterly winds (Fig. 1d), the freshwater bulge
200   shifted westwards and advected offshore around the Modaomen sub-estuary, with the offshore migration of the bloom (Fig.
2r, t) likely driven by anticyclonic circulation (Pan et al. 2014). The Chl a concentrations near the entrances of the three sub-
estuaries remained relatively high (> 10 µg L^{-1}), and the DO concentrations remained at high levels of > 250 µmol kg^{-1}, ~ 20 %
over the saturation levels (Fig. 2s, t).

205   Similar to Leg 1, the surface waters penetrated into the subsurface layer along the coast, likely forced by the downwelling-
favorable winds (Huang et al. 2019), increasing the temperature and DO concentrations and decreasing the salinity, particularly
in the mid-depth layer (Fig. S1). The downward penetration of surface waters, nonetheless, seemed restricted to the ~ 10-m
isobath and thus offset only a limited amount of the oxygen reduction caused by biochemical consumption (Koweek et al.
2020). DO concentrations in the bottom layer were reduced to ~ 46 µmol kg^{-1} off the Maodaomen sub-estuary along the 20-m
210   isobath and to < 94 µmol kg^{-1} to the southwest of Hong Kong (Fig. 2w), indicating the reinstatement of hypoxia. When sites
were revisited on July 31, the reemerging hypoxia was found to have been strengthened, with oxygen levels down to ~ 37
µmol kg^{-1}, and expanded along the 20-m isobaths. It should be noted that the hypoxia formed off the Modaomen sub-estuary
was characterized by a temperature of ~ 28 ℃ during Leg 2, while the oxygen-deficit zone to the southwest of Hong Kong
showed a relatively low temperature of < 27 ℃ (Fig. 2u), likely due to the cross-isobath transport of shelf benthic waters,
215   arising from local topographic effects (Dai et al. 2014, Wang et al. 2014), during Leg 1. In this sense, the lateral advection of

shelf benthic waters is not a prerequisite for the initiation of hypoxia formation off the PRE, but it might contribute to the reinstatement of hypoxia southwest off Hong Kong.

4 Discussion

4.1 Physical controls on the maintenance, destruction and reinstatement of hypoxia

220 A stable water column is a key prerequisite for the formation and maintenance of hypoxia in coastal oceans (Wang and Justić 2009, Obenour et al. 2012, Testa and Kemp 2014, Lu et al. 2018, Zhang et al. 2019), which restricts the oxygen supply by suppressing advective and diffusive mixing with oxygen-rich waters (Murphy et al. 2011, Cui et al. 2019). Many studies have demonstrated that density stratification becomes enhanced and stabilizes subsurface waters when freshwater flows over seawater (Gan et al. 2009, MacCready et al. 2009, Bianchi et al. 2010), allowing oxygen depletion over a longer timescale

225 (Fennel and Testa 2019). Water column stability can be indicated by the buoyancy frequency (also known as the Brunt-Väisälä frequency),

$$N^2 = -(g/\rho)(\partial\rho/\partial z) \qquad (8)$$

where g is the gravitational acceleration, ρ is potential density, and z is the height above the seabed. Generally, a positive N^2 (i.e., $N^2 > 0$) indicates a stable regime where stratification may suppress turbulence (Tedford et al. 2009), and larger N^2 values

230 indicate a more stable water column.

Off the PRE, when not influenced by freshwater inputs the surface layer showed a relatively small N^2 close to 0 (e.g., Station A14, Fig. 4c). However, in the presence of the freshwater plume, the surface layer became more stable, with a larger N^2 of > 1×10^{-3}, or even > 5×10^{-3} (e.g., stations A8 and A11, Fig. 4a, b). It therefore acted as a barrier layer, with weak dissipation of

235 oxygen into the bottom layer (Cui et al. 2019). The inherent pycnocline between the offshore surface water and shelf benthic waters mainly driven by steep temperature gradients (Qu et al. 2007), such as at Station A14, was observable as a second pycnocline in the plume region (e.g., stations A8 and F304, Fig. 4a, d), yet with weaker stratification likely from increased shear stresses in shallower waters (Pan and Gu 2016). This three-layer structure, separated by two pycnoclines, can effectively decrease oxygen influx from the surface and facilitate oxygen depletion in bottom waters.

240

Water column stability largely depends on wind stress (Wilson et al. 2008, Wang and Justić 2009). Higher wind stress usually de-stratifies the water column, leading to stronger turbulent mixing, air-sea gas exchange and reaeration (Chen et al. 2015, Huang et al. 2019), relieving hypoxic conditions (Ni et al. 2016, Wei et al. 2016). During the typhoon period, the wind speed rose to as high as 13 m s^{-1} (Fig. 1c), which was large enough to break the stratification (Geng et al. 2019) driven by freshwater

245 inputs and the inherent thermocline. This mixed high-temperature, low-salinity surface waters and cold, saline bottom waters, resulting in a vertically-homogeneous temperature and salinity, as observed during Leg 2 (Fig. 3). A sudden decrease in Chl a concentrations in the surface layer might be due to dilution from the vertical mixing of surface plume waters with subsurface

Biogeosciences
Discussions

Open Access

seawaters (Qiu et al. 2019). The surface waters became undersaturated (~ 90 % of the oxygen saturation level), also likely due to the upward mixing of low-oxygen waters, which in turn favored the ventilation of bottom waters and the breakdown of

250 hypoxic conditions (Hu et al. 2017). Despite wind speeds still as high as 10 m s^{-1} during Leg 2 (Fig. 1c), stratification was regenerated in the top ~ 10 m of the plume region, which had a relatively high N^2 (Fig. 4e-h) under easterly winds (Fig. 1d). This suggests that freshwater input-induced stratification suppressed turbulent mixing driven by wind stress, favoring the initiation of hypoxia development even under downwelling-favorable conditions. How wind direction ultimately affects the intensity, spatial area, and location of hypoxia needs further study (Scully 2013, Chen et al. 2015, Li et al. 2020).
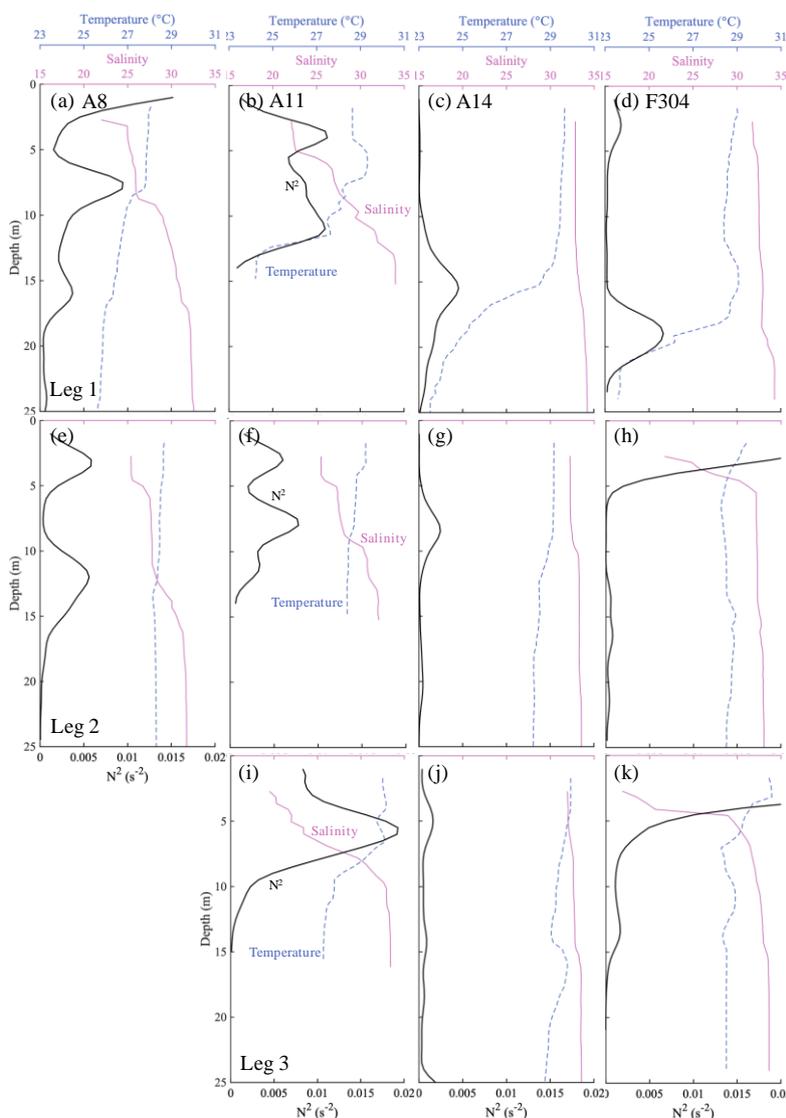
Figure 4: Profiles of temperature (℃) (green dashed lines), salinity (pink solid lines), and buoyancy frequency N^2 (s^{-2}) (bold black solid lines) at stations A8, A11, A14 and F304 (see Fig. 1b), with visits both pre-typhoon (Leg 1) and post-typhoon (Legs 2 and 3). The vertical distributions of N^2 have been smoothed by the Gaussian method.

255

Tidal forcing has been suggested as another factor influencing the stability of the water column and the presence of hypoxia

260 (Luo et al. 2009, Chen et al. 2015). Neap tides facilitate hypoxia formation relative to spring tides (Huang et al. 2019), and thus the intensity and area of hypoxia decreases during spring tides and increases during neap tides (Luo et al. 2009, Chen et al. 2015). In the PRE, the dominant irregular semidiurnal mixed tide has a mean tidal range of 0.86-1.63 m, and a spring tidal range of 3.66 m (Mao et al. 2004). Even on the inner shelf, the spring tidal range can reach ~ 2.5 m (Fig. 1e). Rabouille et al. (2008) demonstrated that tidal mixing could disrupt stratification and break hypoxia. However, the DO concentration outside

265 of the Lingdingyang sub-estuary exhibited a tidal fluctuation and spring-to-neap oscillation, with a maximum neighboring oxygen range only of 0.2 and 0.5 mg L^{-1}, respectively (Cui et al. 2019). Our observations showed the maintenance of hypoxia during Leg 1 and the reinstatement of hypoxic or oxygen-deficient conditions from Leg 2 to Leg 3, both over the transformation from a neap tide to a spring tide (Fig. 1e). The extensive hypoxia observed in summer 2017 also occurred during the transformation from a spring tide to a neap tide (Zhao et al. 2020). Hypoxia off the PRE thus could survive from the spring

270 tides under the conditions of a widespread plume and weak winds. Additionally, the variability of bottom salinity with tidal fluctuations (Fig. 3b) implied an important role of the flood-ebb tidal cycle in the modulation of vertical stratification for the formation and destruction of hypoxia (Chen et al. 2015). However, compared to freshwater inputs and wind mixing, tidal forcing acts as a secondary factor influencing the spatial extent and migration of bottom hypoxia (Luo et al. 2009, Chen et al. 2015, Zhang et al. 2019).

275 **4.2 Quantification of oxygen sinks for hypoxia formation**

Analysis of oxygen budgets based on the mass balance of oxygen and estimates of community/bacterial respiration or nitrification rates using field incubations have been common methods to quantify oxygen sinks under hypoxic conditions (Zhang and Li 2010, Li et al. 2015, Cui et al. 2019). However, the budget analysis of oxygen usually assumes a steady state system (Zhang and Li 2010, Cui et al. 2019), since the change of oxygen over time is much smaller than the oxygen depletion

280 and advection/diffusion fluxes (Cui et al. 2019). The respiration or nitrification rates estimated from (enriched) incubation experiments also merely indicate the OCR under a specific low-oxygen condition at the time of sampling (He et al. 2014, Su et al. 2017). Therefore, the magnitude of net oxygen sinks over time that actually lead to the oxygen decline for hypoxia formation remains unclear.

285 In this study, the net OCR for the reinstatement of bottom water hypoxia could be estimated by the oxygen decline post-typhoon from Leg 2 to Leg 3, on the condition of a precedent restoration of density stratification. The three-endmember mixing scheme for the bottom layer has been elucidated in Zhao et al. (2020) for a similar study area off the PRE along the inner NSCS shelf. Endmember selection and verification for the mixing model are described in the Appendix A. A summary of the end-member values used is listed in Table 1. Considering the requirement of isolation from the atmosphere and minimal effects

290 by photosynthetic production of oxygen for estimating OCR, we selected samples with water depths > 10 m, approximately below the pycnocline and where the surface plume was rarely involved (Fig. 2).

Biogeosciences
Discussions

Table 1: Summary of end-member values adopted in the three-endmember mixing model

Water mass	θ (°C)	Salinity	DIC (μmol kg^{-1})	DO (μmol kg^{-1})
Brackish plume water	28.9 ± 0.4[b]	16.9	1776 ± 29[b]	217.3 ± 1.4[c]
Offshore surface water[a]	29.3 ± 0.1	33.7 ± 0.1	1922 ± 5	194.4 ± 0.3[c]
Upwelled subsurface water[a]	22.5 ± 0.1	34.5 ± 0.0	2022 ± 3	180.9

[a]Endmember values were adopted from Zhao et al. (2020)

[b]Uncertainties were derived from samples collected at the entrance of the PRE

295 [c]Uncertainties were calculated by propagating errors associated with the estimation of oxygen solubility using Benson and Krause (1984)
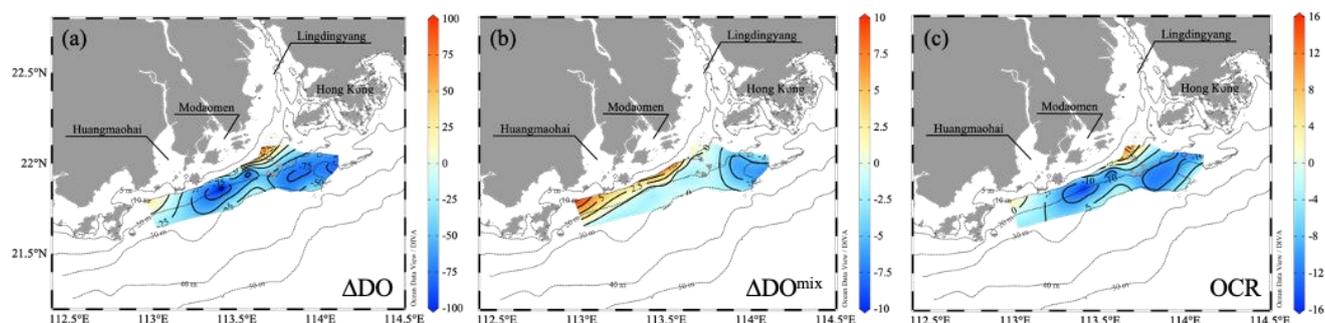

Figure 5: Distribution of (a) total DO changes (ΔDO, μmol kg^{-1}), (b) mixing-induced DO changes (ΔDO^{mix}, μmol kg^{-1}) and (c) the biochemical-induced oxygen consumption rate (OCR, μmol O$_2$ kg^{-1} d^{-1}) between Leg 3 and Leg 2 on the inner NSCS shelf off the PRE.

300

From Leg 2 to Leg 3, DO concentrations in bottom waters were generally reduced by > 25 μmol kg^{-1}, with two hotspots showing reductions up to 75 μmol kg^{-1}: one located offshore of the Lingdingyang sub-estuary, to the southwest of Hong Kong, and the other between the Modaomen and Huangmaohai sub-estuaries (Fig. 5a). The distribution of OCR estimates in bottom waters almost mirrored variations in the total DO pattern from Leg 2 to Leg 3 (Fig. 5a, c). This biochemically-mediated OCR
305 ranged from -0.9 μmol O$_2$ kg^{-1} d^{-1} at offshore non-hypoxic stations to -19.5$\pm$0.4 μmol O$_2$ kg^{-1} d^{-1} in hypoxic waters, with an average of -14.6$\pm$4.8 μmol O$_2$ kg^{-1} d^{-1} in the oxygen-deficit zone. The uncertainty introduced by the mixing scheme is estimated to be 0.63-0.98 μmol O$_2$ kg^{-1} d^{-1}, accounting for a deviation of 4-27 %. It also should be noted that the OCR estimated here is a lower limit, as the actual time that significant oxygen consumption started might be later than our observations during the first half of Leg 2. Additionally, the amount of oxygen supplied from the surface by diffusion, which was greatly inhibited by
310 density stratification (Fig. 4), was assumed negligible.

The shifting from an excess of oxygen sinks over sources during hypoxia formation to a balance between oxygen consumption and replenishment for the maintenance of hypoxia possibly resulted from a decrease in the OCR and/or an increase in the diffusion flux of oxygen. At Station F303, DO declined slowly at a rate of ~ -9 μmol O$_2$ kg^{-1} d^{-1} from July 20-22, when the
315 winds remained strong, and the OCR decreased to ~ -5.5 μmol O$_2$ kg^{-1} d^{-1} from Leg 2 to Leg 3. The continuous oxygen decline

in the high-OCR region would also augment the gradient of oxygen concentrations with respect to surrounding waters (Zhang and Li 2010, Wang et al. 2017), increasing its diffusion flux into the oxygen-deficit or hypoxic zone and gradually offsetting the oxygen consumption. Hypoxia was therefore maintained when the decreasing OCR almost achieved equilibrium with the oxygen supply from turbulence and vertical diffusivity.

320

Shoreward intrusion of oceanic oxygen-undersaturated subsurface waters also acts as a non-local driver on coastal hypoxia by lowering the initial DO concentration (Wang 2009, Qian et al. 2017), which is largely dependent on the source of the subsurface water masses and biogeochemical reactions along the pathway of the intrusion. Although the bottom layer was almost completely occupied by cold, high-salinity oceanic subsurface waters beyond the 20-m isobath during Leg 1 (Fig. 2e), the

325 upwelling signal only re-occurred in waters to the southwest of Hong Kong after disturbance by the typhoon (Fig. 2m, u). Based on the three-endmember mixing model, the mixing-induced DO changes were estimated to average -5.7±0.8 μmol kg^{-1} in bottom waters southwest off Hong Kong, higher than in other regions west of the PRE (e.g. beyond the 20-m isobath; -1.4±0.8 μmol kg^{-1}) (Fig. 5b). This upwelling-induced reduction in the initial DO level amounted to 8.6±1.7 % of the oxygen decline therein, suggesting coastal upwelling played a minor role in hypoxia formation when compared to biochemical oxygen

330 consumption.

The above estimated OCR and the contribution of shoreward-intruded shelf benthic waters made it possible to roughly estimate the hypoxia timescale: i.e., the time that the DO level in a known volume of water takes to decrease below the hypoxia threshold from an assumed initial DO concentration (Fennel and Testa 2019). In this study, for the reinstatement of hypoxia after the

335 typhoon, the initial DO level in subsurface waters could be taken as ~ 180 μmol kg^{-1}, which varied slightly throughout the time-series observations (Fig. 3c). Considering the OCR for the hypoxic zone was at most ~ -20 μmol O$_2$ kg^{-1} d^{-1}, and the negligible contribution of lateral advection to oxygen loss off the Modaomen sub-estuary, it took nearly 6 days for the drawdown of DO to reach concentrations of ~ 63 μmol kg^{-1} within a limited area. Scaling to a larger area, it would instead take 8-12 days if we choose the average OCR of the oxygen-deficient zone, ~ -15±5 μmol O$_2$ kg^{-1} d^{-1}. The closeness of these

340 estimates with the water residence time (~ 15 days (Li et al. 2020)) could partly explain the occurrence of periodic hypoxia to the west off the PRE (Su et al. 2017, Zhao et al. 2020).

For the more common scenario of hypoxia formed during the late spring, the initial DO level was estimated to be ~ 183 μmol kg^{-1}, assuming that the bottom layer on the shelf was occupied by well-oxygenated offshore surface waters before shoreward

345 intrusion of oxygen-deficient offshore subsurface waters. The hypoxia hotspot will then first occur ~ 6 days after its initiation on the inner NSCS shelf off the PRE. This result is at the lower end of the hypoxia timescale in large estuaries and river-dominated shelves globally, which varies from several days to as long as 1500 days for hypoxia to develop once initiated (Fennel and Testa 2019).

4.3 Imprint of tropical cyclones on the evolution of coastal hypoxia in a changing climate

350   Tropical cyclones dramatically alter the physical stability of the water column and attenuate or even disrupt hypoxic conditions at low and mid-latitudes, such as off the Changjiang Estuary (Ni et al. 2016) and the PRE (Su et al. 2017, Huang et al. 2019), in Chesapeake Bay (Testa and Kemp 2014, Testa et al. 2017) and the northern Gulf of Mexico (Wang and Justić 2009, Feng et al. 2012). These intense, episodic storms thus strongly impact the duration and intensity of oxygen depletion in coastal bottom waters (Rabalais et al. 2009, Wang et al. 2017), driving the seasonal hypoxia to be intermittent. As shown in Fig. 1, at

355   least four named tropical cyclones impacted the study area from May to August in 2018, most of which shifted the wind direction to easterly or southeasterly and increased the wind speed up to 10 m s^{-1}. This was not an exception, as annually there have been ~ 6 tropical cyclones travelling across the NSCS from May to September, when seasonal hypoxia develops (Qian et al. 2018, Wang et al. 2018), during the period from 1975-2019 (Fig. 6a). About five of the six annual tropical cyclones, on average, had the potential to overwhelmingly destroy the stability of the water column and replenish the bottom waters with

360   oxygen. Indeed, when tropical cyclones have impacted the NSCS over the last four decades, the local maximum wind speeds typically reached over 10 m s^{-1}, and often were larger than 15 m s^{-1} (Fig. 6b). The wind direction was inclined to be from the south, varying between southeasterly and southwesterly (Fig. 6c) depending on the trajectory of the tropical cyclone (Rabalais et al. 2007). The southerly winds were more likely to confine the river plume to the coast (Xu et al. 2019) and even force the riverine freshwater to subduct down to the deep (Fig. S1), strengthening the reaeration of the oxygen-poor bottom waters

365   (Wang et al. 2017, Wang et al. 2018, Huang et al. 2019). Therefore, frequent disturbance by tropical cyclones might be one of the vital controls on the intermittent hypoxia in low-latitude river-dominated ocean margins.

In addition to subduing hypoxia, tropical cyclones further contribute to the development of extensive oxygen depletion after the transient dissipation of hypoxia (Rabalais et al. 2009). Heavy precipitation delivered by storms increases riverine freshwater

370   loading to the coastal ocean (Zhou et al. 2012), resulting in intensified stratification when winds weaken (Wilson et al. 2008, Su et al. 2017). Via enhanced vertical mixing and freshwater discharge, large supplies of nutrients to the surface layer fuel phytoplankton blooms following large storms (Zhao et al. 2009, Ni et al. 2016, Wang et al. 2017). The fresh autochthonous organic matter, together with the resuspended sedimentary organic carbon, provides sufficient substrates for microbial respiration in a stratified water column, leading to renewed and exacerbated bottom water oxygen depletion (Zhou et al. 2012,

375   Song et al. 2020). In fact, lowered DO concentrations have been observed after storms along the east coast of North America (Paerl et al. 2000, Tomasko et al. 2006). Hypoxia was re-established across a larger area when Hurricane Katrina crossed the southeast Louisiana coast (Rabalais et al. 2009). Here, off the PRE, we also found that hypoxia re-occurred in the wake of a more extensive freshwater plume and enhanced eutrophication after the passage of typhoon SONTIHN. We would further expect it to develop into more severe hypoxia compared to that found initially during Leg 1, up until the passage of the next

380   storm, Typhoon BEBINCA (Fig. 2d), given that the net OCR maintained a relatively high level after Leg 3.
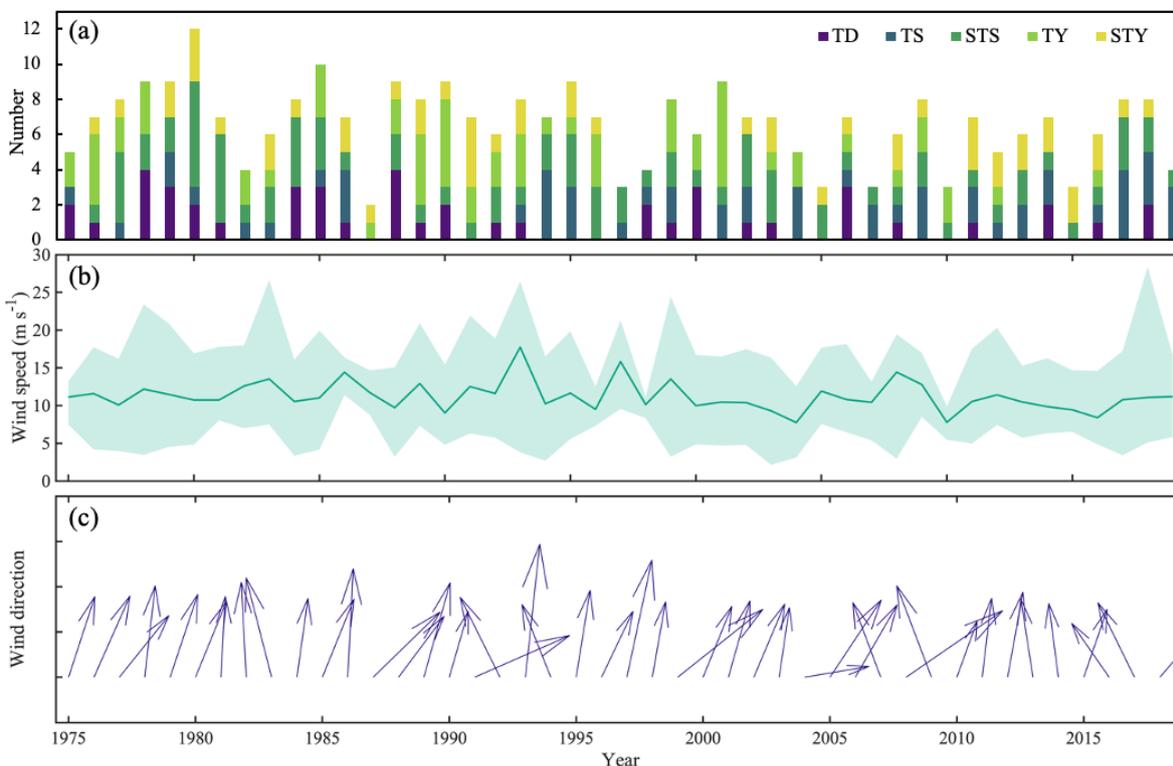
Figure 6: (a) Number of tropical cyclones that impacted the NSCS from May to September, 1975-2019. TD, TS, STS, TY and STY represent tropical depressions (the maximum wind speed near the center is between 10.8-17.1 m s^{-1} over its lifetime), tropical storms (17.2-24.4 m s^{-1}), strong tropical storms (24.5-32.6 m s^{-1}), typhoons (32.7-41.4 m s^{-1}) and strong typhoons (41.5-50.9 m s^{-1}), respectively. (b) The annual average (green solid line) and range (light green shadow) of the maximum wind speed and (c) the annual average wind direction recorded at the Waglan Island station when tropical cyclones impacted the NSCS from 1975-2019.

The exacerbation of coastal hypoxia continues in terms of its intensity, size and frequency in a changing climate (Diaz and Rosenberg 2008, Breitburg et al. 2018) with increased anthropogenic nutrient loadings (Rabalais et al. 2009, Seitzinger et al. 2010, Rabalais et al. 2014). Ocean warming, with an accelerated rate in coastal seas and estuaries, has the potential to mediate the severity of hypoxia via hydrography, nutrient dynamics and/or metabolic effects (Altieri and Gedan 2015). The lower solubility of oxygen and the increased metabolism of marine organisms in warmer waters (Brown et al. 2004, Vázquez-Domínguez et al. 2007) would shorten the length of time to establish hypoxia once initiated, especially coinciding with climate-driven intensification of density stratification (Coma et al. 2009, Rabalais et al. 2010, Murphy et al. 2011), which might lead to a prolonged duration of hypoxia occurrence and an enlarged hypoxic spatial extent with increasing severity. The contribution to the oxygen loss from the lateral advection of subsurface waters might yet become less significant due to the deoxygenation of oceanic waters (Schmidtko et al. 2017). Tropical cyclone activity due to climatic changes is expected to shift towards stronger storms but with a decreasing trend in frequency (Knutson et al. 2010). The less-frequent disturbance in the stability

16

400 of the water column by tropical cyclones favors more persistent hypoxia, and the increases in precipitation during each individual storm are likely to aggravate hypoxia through intensified stratification and nutrient loading (Sinha et al. 2017). However, the increase in intensity of storms may cause more thorough destruction of hypoxia, making predictions of the extent and severity of the reinstated hypoxia more difficult. In this sense, tropical cyclones may have the potential to accelerate the exacerbation of coastal hypoxia in a warmer ocean.

5 Conclusions

We have demonstrated the evolution of intermittent hypoxia in summertime as disturbed by typhoon passage on the inner NSCS shelf off the PRE and examined the controls on formation and maintenance of hypoxia in this dynamic river-dominated marginal system. Eutrophication-induced hypoxia off the PRE was exacerbated with an enlarged area of ~ 660 km^2 and the lowest ever regional DO concentration of 3.5 μmol kg^{-1} (~ 0.1 mg L^{-1}). Turbulent mixing driven by wind stress and/or tidal

410 forcing was largely suppressed by freshwater input-induced stratification, which stabilized the water column, restricted the ventilation of the subsurface water and facilitated the formation and maintenance of hypoxia. We estimated for the first time the *in situ* OCR over the destruction and reinstatement of hypoxia, which took place on a time scale of 6-12 d. This hypoxia timescale is comparable with water residence time and the disturbance of hypoxia from frequent tropical cyclones or high-wind events throughout the summer season, which could largely explain the intermittent nature of hypoxia off the PRE.

415 Through intensified stratification and nutrient loading by increased precipitation and river discharge during individual storm, tropical cyclones might accelerate the exacerbation of coastal hypoxia with a longer duration and stronger intensity in a warmer ocean in the future.

Appendix A: Verification and endmember selection for the three-endmember mixing model

The potential temperature – salinity diagram is shown in Fig. S2a. We adopted the endmember values of offshore surface water

420 and upwelled subsurface water from Zhao et al. (2020), as our sampling was limited almost exclusively within the 30-m isobaths (Fig. 1b) and these values were consistent with those found in previous studies (Cao et al. 2011, Guo and Wong 2015, Su et al. 2017). The brackish plume water was assumed to partly subduct to the bottom layer when it was attached to the coast constrained by easterly winds. The endmember values of brackish plume water were thus determined from the surface water samples near the mouth of the PRE with a salinity of ~ 16.9, mainly consisting of a mixture of riverine freshwater and offshore

425 surface water. The DIC endmember of brackish plume water here was consistent with the predicted value using the endmember values of riverine/plume water reported by Su et al. (2017), whereas it was higher than that calculated by using the endmember values of riverine freshwater from Zhao et al. (2020) since the riverine DIC concentrations might be diluted by abnormally high river discharge in 2017 (Guo et al. 2008). For simplification, DO concentrations in offshore surface water were assumed to be saturated, in equilibrium with the atmosphere, while the upwelled subsurface water was assumed oxygen-deficient by ~

430 16% relative to the saturation level. The DO endmember value of brackish plume water was also assumed to be equilibrated with the atmosphere, probably because the biological productivity was largely limited by high turbidity in shallow waters near the mouth of the PRE. The predicted quasi-conservative TA ($TA^{pre} = TA_{PW} \times f_{RW} + TA_{SW} \times f_{SW} + TA_{SUB} \times f_{SUB}$; same for DIC^{pre}) is mostly consistent with measured values (Fig. S2b), with a subtle difference of 8 ± 8 µmol kg^{-1} likely caused by measurement errors, computational errors in the mixing scheme and/or biological processes. The slope of ΔDIC ($\Delta DIC = DIC^{meas} - DIC^{pre}$)

435 vs. ΔDO in bottom waters was -0.93 ± 0.07 (Fig. S2c), similar to that reported by Zhao et al. (2020).

Data Availability. Data for temperature, salinity, DO and Chl *a* are currently for review and will be available at National Earth System Science Data Sharing Infrastructure, National Science & Technology Infrastructure of China (http://www.geodata.cn) with DOI. DOI number will be provided before the acceptance of this manuscript. The wind speeds

440 and directions at the Waglan Island from May to August, 2018 were obtained from the Hong Kong Observatory (http://www.hko.gov.hk/tc/cis/climat.htm). The tidal heights at the Dawanshan gauge station near the Station F303 from May to August, 2018 were downloaded from the website (http://www.chinaports.com/tidal/). Information from the tropical cyclone database (1949-2019) was obtained from the China Meteorological Administration (http://tcdata.typhoon.org.cn/).

445 **Supplement**. Additional figures referenced in text: **Figure S1**. Distribution of temperature, salinity, DO and Chl *a* concentrations in the middle layer off the PRE during Leg 1 prior to Typhoon, and during Legs 2 and 3 post-typhoon; **Figure S2**. (a) Potential temperature vs. salinity, (b) predicted TA vs. measured TA, and (c) ΔDIC vs. ΔDO on the NSCS shelf off the PRE.

450 **Competing interests**. The authors declare that they have no conflict of interest.

Author contribution. YZ and MD are major contributors to the study's conception, data analysis and drafting the paper. KU contributed the sample collection and measurements of DO data. ZL contributed substantially to sample collections and data analysis of physical forcing. HL provided Chl *a* data, and JG provided CTD data. YL, JL, and FM also contributed significantly

455 to cruise design, sample collections and/or data acquisition.

Biogeosciences
Discussions
Open Access
EGU

References

465   Allahdadi, M. N. and Li, C.: Numerical Experiment of Stratification Induced by Diurnal Solar Heating Over the Louisiana Shelf, in: Modeling Coastal Hypoxia: Numerical Simulations of Patterns, Controls and Effects of Dissolved Oxygen Dynamics, edited by: Justic, D., Rose, K. A., Hetland, R. D. and Fennel, K., Springer International Publishing, Cham, 1-22, doi:10.1007/978-3-319-54571-4_1, 2017.

470   Altieri, A. H. and Gedan, K. B.: Climate change and dead zones, Global Change Biol, 21, 1395-1406, doi:10.1111/gcb.12754, 2015.

Benson, B. B. and Krause Jr, D.: The concentration and isotopic fractionation of oxygen dissolved in freshwater and seawater in equilibrium with the atmosphere1, Limnol Oceanogr, 29, 620-632, doi:10.4319/lo.1984.29.3.0620, 1984.
475

Bianchi, T. S., Dimarco, S. F., Cowan, J. H., Hetland, R. D., Chapman, P., Day, J. W. and Allison, M. A.: The science of hypoxia in the northern Gulf of Mexico: A review, Sci Total Environ, 408, 1471-1484, doi:10.1016/j.scitotenv.2009.11.047, 2010.

480   Breitburg, D., Levin, L. A., Oschlies, A., Grégoire, M., Chavez, F. P., Conley, D. J., Garçon, V., Gilbert, D., Gutiérrez, D., Isensee, K., Jacinto, G. S., Limburg, K. E., Montes, I., Naqvi, S. W. A., Pitcher, G. C., Rabalais, N. N., Roman, M. R., Rose, K. A., Seibel, B. A., Telszewski, M., Yasuhara, M. and Zhang, J.: Declining oxygen in the global ocean and coastal waters, Science, 359, eaam7240, doi:10.1126/science.aam7240, 2018.

485   Brown, J. H., Gillooly, J. F., Allen, A. P., Savage, V. M. and West, G. B.: Toward a metabolic theory of ecology, Ecology, 85, 1771-1789, doi:10.1890/03-9000, 2004.

Cai, W.-J., Hu, X., Huang, W.-J., Jiang, L.-Q., Wang, Y., Peng, T.-H. and Zhang, X.: Alkalinity distribution in the western North Atlantic Ocean margins, Journal of Geophysical Research: Oceans, 115, doi:10.1029/2009JC005482, 2010.
490

Cai, W. J., Dai, M. H., Wang, Y. C., Zhai, W. D., Huang, T., Chen, S. T., Zhang, F., Chen, Z. Z. and Wang, Z. H.: The biogeochemistry of inorganic carbon and nutrients in the Pearl River estuary and the adjacent Northern South China Sea, Cont Shelf Res, 24, 1301-1319, doi:10.1016/j.csr.2004.04.005, 2004.

495   Cao, Z. M., Dai, M. H., Zheng, N., Wang, D. L., Li, Q., Zhai, W. D., Meng, F. F. and Gan, J. P.: Dynamics of the carbonate system in a large continental shelf system under the influence of both a river plume and coastal upwelling, J Geophys Res-Biogeo, 116, G02010, doi:10.1029/2010jg001596, 2011.

Chen, X., Shen, Z., Li, Y. and Yang, Y.: Physical controls of hypoxia in waters adjacent to the Yangtze Estuary: A numerical
500   modeling study, Mar Pollut Bull, 97, 349-364, doi:10.1016/j.marpolbul.2015.05.067, 2015.

Chen, X., Shen, Z., Li, Y. and Yang, Y.: Tidal modulation of the hypoxia adjacent to the Yangtze Estuary in summer, Mar Pollut Bull, 100, 453-463, doi:10.1016/j.marpolbul.2015.08.005, 2015.

505   Chen, Z., Gong, W., Cai, H., Chen, Y. and Zhang, H.: Dispersal of the Pearl River plume over continental shelf in summer, Estuarine, Coastal and Shelf Science, 194, 252-262, doi:10.1016/j.ecss.2017.06.025, 2017.

Chen, Z., Pan, J., Jiang, Y. and Lin, H.: Far-reaching transport of Pearl River plume water by upwelling jet in the northeastern South China Sea, J Marine Syst, 173, 60-69, doi:10.1016/j.jmarsys.2017.04.008, 2017.
510

Coma, R., Ribes, M., Serrano, E., Jiménez, E., Salat, J. and Pascual, J.: Global warming-enhanced stratification and mass mortality events in the Mediterranean, Proceedings of the National Academy of Sciences, 106, 6176, doi:10.1073/pnas.0805801106, 2009.

515   Cui, Y. S., Wu, J. X., Ren, J. and Xu, J.: Physical dynamics structures and oxygen budget of summer hypoxia in the Pearl River Estuary, Limnol Oceanogr, 64, 131-148, doi:10.1002/lno.11025, 2019.

Dai, M., Gan, J., Han, A., Kung, H. and Yin, Z.: Physical dynamics and biogeochemistry of the Pearl River plume, in: Biogeochemical Dynamics at Major River-Coastal Interfaces: Linkages with Global Change, edited by: Bianchi, T. S., Allison, 520   M. and Cai, W.-J., Cambridge University Press, Cambridge, 321-352, 2014.

Diaz, R. J. and Rosenberg, R.: Spreading Dead Zones and Consequences for Marine Ecosystems, Science, 321, 926, doi:10.1126/science.1156401, 2008.

525   Feng, Y., Dimarco, S. F. and Jackson, G. A.: Relative role of wind forcing and riverine nutrient input on the extent of hypoxia in the northern Gulf of Mexico, Geophys Res Lett, 39, doi:10.1029/2012GL051192, 2012.

Fennel, K. and Testa, J. M.: Biogeochemical Controls on Coastal Hypoxia, Annual Review of Marine Science, 11, 105-130, doi:10.1146/annurev-marine-010318-095138, 2019.
530
Gan, J., Cheung, A., Guo, X. and Li, L.: Intensified upwelling over a widened shelf in the northeastern South China Sea, Journal of Geophysical Research: Oceans, 114, doi:10.1029/2007JC004660, 2009.

Gan, J. P., Li, L., Wang, D. X. and Guo, X. G.: Interaction of a river plume with coastal upwelling in the northeastern South 535   China Sea, Cont Shelf Res, 29, 728-740, doi:10.1016/j.csr.2008.12.002, 2009.

Geng, B. X., Xiu, P., Shu, C., Zhang, W. Z., Chai, F., Li, S. Y. and Wang, D. X.: Evaluating the Roles of Wind- and Buoyancy Flux-Induced Mixing on Phytoplankton Dynamics in the Northern and Central South China Sea, J Geophys Res-Oceans, 124, 680-702, doi:10.1029/2018jc014170, 2019.
540
Gilbert, D., Rabalais, N. N., Díaz, R. J. and Zhang, J.: Evidence for greater oxygen decline rates in the coastal ocean than in the open ocean, Biogeosciences, 7, 2283-2296, doi:10.5194/bg-7-2283-2010, 2010.

Guo, X. H., Cai, W. J., Zhai, W. D., Dai, M. H., Wang, Y. C. and Chen, B. S.: Seasonal variations in the inorganic carbon 545   system in the Pearl River (Zhujiang) estuary, Cont Shelf Res, 28, 1424-1434, doi:10.1016/j.csr.2007.07.011, 2008.

Guo, X. H. and Wong, G. T. F.: Carbonate chemistry in the Northern South China Sea Shelf-sea in June 2010, Deep-Sea Res Pt Ii, 117, 119-130, doi:10.1016/j.dsr2.2015.02.024, 2015.

550   He, B. Y., Dai, M. H., Zhai, W. D., Guo, X. H. and Wang, L. F.: Hypoxia in the upper reaches of the Pearl River Estuary and its maintenance mechanisms: A synthesis based on multiple year observations during 2000-2008, Mar Chem, 167, 13-24, doi:10.1016/j.marchem.2014.07.003, 2014.

Hu, X. P., Li, Q., Huang, W. J., Chen, B. S., Cai, W. J., Rabalais, N. N. and Turner, R. E.: Effects of eutrophication and benthic 555   respiration on water column carbonate chemistry in a traditional hypoxic zone in the Northern Gulf of Mexico, Mar Chem, 194, 33-42, doi:10.1016/j.marchem.2017.04.004, 2017.

Huang, J., Hu, J., Li, S., Wang, B., Xu, Y., Liang, B. and Liu, D.: Effects of Physical Forcing on Summertime Hypoxia and Oxygen Dynamics in the Pearl River Estuary, Water-Sui, 11, 2080, 2019.
560

Knutson, T. R., Mcbride, J. L., Chan, J., Emanuel, K., Holland, G., Landsea, C., Held, I., Kossin, J. P., Srivastava, A. K. and Sugi, M.: Tropical cyclones and climate change, Nat Geosci, 3, 157-163, doi:10.1038/ngeo779, 2010.

565   Koweek, D. A., García-Sánchez, C., Brodrick, P. G., Gassett, P. and Caldeira, K.: Evaluating hypoxia alleviation through induced downwelling, Sci Total Environ, 719, 137334, doi:10.1016/j.scitotenv.2020.137334, 2020.

Labasque, T., Chaumery, C., Aminot, A. and Kergoat, G.: Spectrophotometric Winkler determination of dissolved oxygen: re-examination of critical factors and reliability, Mar Chem, 88, 53-60, doi:10.1016/j.marchem.2004.03.004, 2004.

570   Laurent, A. and Fennel, K.: Time-Evolving, Spatially Explicit Forecasts of the Northern Gulf of Mexico Hypoxic Zone, Environ Sci Technol, doi:10.1021/acs.est.9b05790, 2019.

Li, D., Gan, J., Hui, R., Liu, Z., Yu, L., Lu, Z. and Dai, M.: Vortex and Biogeochemical Dynamics for the Hypoxia Formation Within the Coastal Transition Zone off the Pearl River Estuary, Journal of Geophysical Research: Oceans, 125, 575   e2020JC016178, doi:10.1029/2020JC016178, 2020.

Li, M., Lee, Y. J., Testa, J. M., Li, Y., Ni, W., Kemp, W. M. and Di Toro, D. M.: What drives interannual variability of hypoxia in Chesapeake Bay: Climate forcing versus nutrient loading?, Geophys Res Lett, 43, 2127-2134, doi:10.1002/2015GL067334, 2016.

580   Li, X. F., Xu, J., Shi, Z. and Li, R. H.: Response of Bacterial Metabolic Activity to the River Discharge in the Pearl River Estuary: Implication for CO2 Degassing Fluxes, Front Microbiol, 10, 1026, doi:10.3389/fmicb.2019.01026, 2019.

Li, Y., Li, M. and Kemp, W. M.: A Budget Analysis of Bottom-Water Dissolved Oxygen in Chesapeake Bay, Estuar Coast, 585   38, 2132-2148, doi:10.1007/s12237-014-9928-9, 2015.

Lu, Z. M. and Gan, J. P.: Controls of seasonal variability of phytoplankton blooms in the Pearl River Estuary, Deep-Sea Res Pt Ii, 117, 86-96, doi:10.1016/j.dsr2.2013.12.011, 2015.

590   Lu, Z. M., Gan, J. P., Dai, M. H., Liu, H. B. and Zhao, X. Z.: Joint Effects of Extrinsic Biophysical Fluxes and Intrinsic Hydrodynamics on the Formation of Hypoxia West off the Pearl River Estuary, J Geophys Res-Oceans, 123, 6241-6259, doi:10.1029/2018jc014199, 2018.

Luo, L., Li, S. and Wang, D.: Hypoxia in the Pearl River Estuary, the South China Sea, in July 1999, Aquat Ecosyst Health, 595   12, 418-428, doi:10.1080/14634980903352407, 2009.

Maccready, P., Banas, N. S., Hickey, B. M., Dever, E. P. and Liu, Y.: A model study of tide- and wind-induced mixing in the Columbia River Estuary and plume, Cont Shelf Res, 29, 278-291, doi:10.1016/j.csr.2008.03.015, 2009.

600   Mao, Q. W., Shi, P., Yin, K. D., Gan, J. P. and Qi, Y. Q.: Tides and tidal currents in the Pearl River estuary, Cont Shelf Res, 24, 1797-1808, doi:10.1016/j.csr.2004.06.008, 2004.

Mendelsohn, R., Emanuel, K., Chonabayashi, S. and Bakkensen, L.: The impact of climate change on global tropical cyclone damage, Nat Clim Change, 2, 205-209, doi:10.1038/Nclimate1357, 2012.

605

Murphy, R. R., Kemp, W. M. and Ball, W. P.: Long-Term Trends in Chesapeake Bay Seasonal Hypoxia, Stratification, and Nutrient Loading, Estuar Coast, 34, 1293-1309, doi:10.1007/s12237-011-9413-7, 2011.

Naqvi, S. W. A., Bange, H. W., Farías, L., Monteiro, P. M. S., Scranton, M. I. and Zhang, J.: Marine hypoxia/anoxia as a 610   source of CH4 and N2O, Biogeosciences, 7, 2159-2190, doi:10.5194/bg-7-2159-2010, 2010.

Ni, X., Huang, D., Zeng, D., Zhang, T., Li, H. and Chen, J.: The impact of wind mixing on the variation of bottom dissolved oxygen off the Changjiang Estuary during summer, J Marine Syst, 154, 122-130, doi:10.1016/j.jmarsys.2014.11.010, 2016.

615   Obenour, D. R., Michalak, A. M., Zhou, Y. and Scavia, D.: Quantifying the Impacts of Stratification and Nutrient Loading on Hypoxia in the Northern Gulf of Mexico, Environ Sci Technol, 46, 5489-5496, doi:10.1021/es204481a, 2012.

Paerl, H. W., Bales, J. D., Ausley, L. W., Buzzelli, C. P., Crowder, L. B., Eby, L. A., Go, M., Peierls, B. L., Richardson, T. L. and Ramus, J. S.: Hurricanes' hydrological, ecological effects linger in major U.S. estuary, Eos, Transactions American
620   Geophysical Union, 81, 457-462, doi:10.1029/00EO00338, 2000.

Pan, J. Y. and Gu, Y. Z.: Cruise observation and numerical modeling of turbulent mixing in the Pearl River estuary in summer, Cont Shelf Res, 120, 122-138, doi:10.1016/j.csr.2016.03.019, 2016.

625   Pan, J. Y., Gu, Y. Z. and Wang, D. X.: Observations and numerical modeling of the Pearl River plume in summer season, J Geophys Res-Oceans, 119, 2480-2500, doi:10.1002/2013jc009042, 2014.

Qian, W., Dai, M., Xu, M., Kao, S.-J., Du, C., Liu, J., Wang, H., Guo, L. and Wang, L.: Non-local drivers of the summer hypoxia in the East China Sea off the Changjiang Estuary, Estuarine, Coastal and Shelf Science, 198, 393-399,
630   doi:10.1016/j.ecss.2016.08.032, 2017.

Qian, W., Gan, J. P., Liu, J. W., He, B. Y., Lu, Z. M., Guo, X. H., Wang, D. L., Guo, L. G., Huang, T. and Dai, M. H.: Current status of emerging hypoxia in a eutrophic estuary: The lower reach of the Pearl River Estuary, China, Estuar Coast Shelf S, 205, 58-67, doi:10.1016/j.ecss.2018.03.004, 2018.
635
Qiu, D., Zhong, Y., Chen, Y., Tan, Y., Song, X. and Huang, L.: Short-Term Phytoplankton Dynamics During Typhoon Season in and Near the Pearl River Estuary, South China Sea, Journal of Geophysical Research: Biogeosciences, 124, 274-292, doi:10.1029/2018JG004672, 2019.

640   Qu, T., Du, Y., Gan, J. and Wang, D.: Mean seasonal cycle of isothermal depth in the South China Sea, Journal of Geophysical Research: Oceans, 112, doi:10.1029/2006JC003583, 2007.

Rabalais, N. N., Cai, W. J., Carstensen, J., Conley, D. J., Fry, B., Hu, X. P., Quinones-Rivera, Z., Rosenberg, R., Slomp, C. P., Turner, R. E., Voss, M., Wissel, B. and Zhang, J.: Eutrophication-Driven Deoxygenation in the Coastal Ocean, Oceanography,
645   27, 172-183, doi:DOI 10.5670/oceanog.2014.21, 2014.

Rabalais, N. N., Díaz, R. J., Levin, L. A., Turner, R. E., Gilbert, D. and Zhang, J.: Dynamics and distribution of natural and human-caused hypoxia, Biogeosciences, 7, 585-619, doi:10.5194/bg-7-585-2010, 2010.

650   Rabalais, N. N., Turner, R. E., Diaz, R. J. and Justic, D.: Global change and eutrophication of coastal waters, Ices J Mar Sci, 66, 1528-1537, doi:10.1093/icesjms/fsp047, 2009.

Rabalais, N. N., Turner, R. E., Sen Gupta, B. K., Boesch, D. F., Chapman, P. and Murrell, M. C.: Hypoxia in the northern Gulf of Mexico: Does the science support the Plan to Reduce, Mitigate, and Control Hypoxia?, Estuar Coast, 30, 753-772,
655   doi:10.1007/BF02841332, 2007.

Rabouille, C., Conley, D. J., Dai, M. H., Cai, W. J., Chen, C. T. A., Lansard, B., Green, R., Yin, K., Harrison, P. J., Dagg, M. and Mckee, B.: Comparison of hypoxia among four river-dominated ocean margins: The Changjiang (Yangtze), Mississippi, Pearl, and Rhône rivers, Cont Shelf Res, 28, 1527-1537, doi:10.1016/j.csr.2008.01.020, 2008.
660

Schmidtko, S., Stramma, L. and Visbeck, M.: Decline in global oceanic oxygen content during the past five decades, Nature, 542, 335-339, doi:10.1038/nature21399, 2017.

Scully, M. E.: Physical controls on hypoxia in Chesapeake Bay: A numerical modeling study, Journal of Geophysical Research: Oceans, 118, 1239-1256, doi:10.1002/jgrc.20138, 2013.

665

Seitzinger, S. P., Mayorga, E., Bouwman, A. F., Kroeze, C., Beusen, A. H. W., Billen, G., Van Drecht, G., Dumont, E., Fekete, B. M., Garnier, J. and Harrison, J. A.: Global river nutrient export: A scenario analysis of past and future trends, Global Biogeochem Cy, 24, doi:10.1029/2009GB003587, 2010.

670

Sinha, E., Michalak, A. M. and Balaji, V.: Eutrophication will increase during the 21st century as a result of precipitation changes, Science, 357, 405, doi:10.1126/science.aan2409, 2017.

Song, G., Zhao, L., Chai, F., Liu, F., Li, M. and Xie, H.: Summertime Oxygen Depletion and Acidification in Bohai Sea, China, Front Mar Sci, 7, doi:10.3389/fmars.2020.00252, 2020.

675

Su, J.: Overview of the South China Sea circulation and its influence on the coastal physical oceanography outside the Pearl River Estuary, Cont Shelf Res, 24, 1745-1760, doi:10.1016/j.csr.2004.06.005, 2004.

Su, J. Z., Dai, M. H., He, B. Y., Wang, L. F., Gan, J. P., Guo, X. H., Zhao, H. D. and Yu, F. L.: Tracing the origin of the oxygen-consuming organic matter in the hypoxic zone in a large eutrophic estuary: the lower reach of the Pearl River Estuary, China, Biogeosciences, 14, 4085-4099, doi:10.5194/bg-14-4085-2017, 2017.

680

Tedford, E. W., Carpenter, J. R., Pawlowicz, R., Pieters, R. and Lawrence, G. A.: Observation and analysis of shear instability in the Fraser River estuary, Journal of Geophysical Research: Oceans, 114, doi:10.1029/2009JC005313, 2009.

685

Testa, J. M., Clark, J. B., Dennison, W. C., Donovan, E. C., Fisher, A. W., Ni, W., Parker, M., Scavia, D., Spitzer, S. E., Waldrop, A. M., Vargas, V. M. D. and Ziegler, G.: Ecological Forecasting and the Science of Hypoxia in Chesapeake Bay, Bioscience, 67, 614-626, doi:10.1093/biosci/bix048, 2017.

690

Testa, J. M. and Kemp, W. M.: Spatial and Temporal Patterns of Winter–Spring Oxygen Depletion in Chesapeake Bay Bottom Water, Estuar Coast, 37, 1432-1448, doi:10.1007/s12237-014-9775-8, 2014.

Tomasko, D. A., Anastasiou, C. and Kovach, C.: Dissolved oxygen dynamics in Charlotte Harbor and its contributing watershed, in response to hurricanes Charley, Frances, and Jeanne—Impacts and recovery, Estuar Coast, 29, 932-938, doi:10.1007/BF02798653, 2006.

695

Vaquer-Sunyer, R. and Duarte, C. M.: Thresholds of hypoxia for marine biodiversity, Proceedings of the National Academy of Sciences, 105, 15452, doi:10.1073/pnas.0803833105, 2008.

700

Vázquez-Domínguez, E., Vaqué, D. and Gasol, J. M.: Ocean warming enhances respiration and carbon demand of coastal microbial plankton, Global Change Biol, 13, 1327-1334, doi:10.1111/j.1365-2486.2007.01377.x, 2007.

Wang, B.: Hydromorphological mechanisms leading to hypoxia off the Changjiang estuary, Mar Environ Res, 67, 53-58, doi:10.1016/j.marenvres.2008.11.001, 2009.

705

Wang, B., Chen, J. F., Jin, H. Y., Li, H. L., Huang, D. J. and Cai, W. J.: Diatom bloom-derived bottom water hypoxia off the Changjiang estuary, with and without typhoon influence, Limnol Oceanogr, 62, 1552-1569, doi:10.1002/lno.10517, 2017.

710   Wang, B., Hu, J. T., Li, S. Y. and Liu, D. H.: A numerical analysis of biogeochemical controls with physical modulation on hypoxia during summer in the Pearl River estuary, Biogeosciences, 14, 2979-2999, doi:10.5194/bg-14-2979-2017, 2017.

Wang, B., Hu, J. T., Li, S. Y., Yu, L. Q. and Huang, J.: Impacts of anthropogenic inputs on hypoxia and oxygen dynamics in the Pearl River estuary, Biogeosciences, 15, 6105-6125, doi:10.5194/bg-15-6105-2018, 2018.

715

Wang, D. X., Shu, Y. Q., Xue, H. J., Hu, J. Y., Chen, J., Zhuang, W., Zu, T. T. and Xu, J. D.: Relative contributions of local wind and topography to the coastal upwelling intensity in the northern South China Sea, J Geophys Res-Oceans, 119, 2550-2567, doi:10.1002/2013jc009172, 2014.

720   Wang, L. and Justić, D.: A modeling study of the physical processes affecting the development of seasonal hypoxia over the inner Louisiana-Texas shelf: Circulation and stratification, Cont Shelf Res, 29, 1464-1476, doi:10.1016/j.csr.2009.03.014, 2009.

Wei, X., Zhan, H. G., Ni, P. T. and Cai, S. Q.: A model study of the effects of river discharges and winds on hypoxia in summer 725   in the Pearl River Estuary, Mar Pollut Bull, 113, 414-427, doi:10.1016/j.marpolbul.2016.10.042, 2016.

Welschmeyer, N. A.: Fluorometric analysis of chlorophyll a in the presence of chlorophyll b and pheopigments, Limnol Oceanogr, 39, 1985-1992, doi:10.4319/lo.1994.39.8.1985, 1994.

730   Wilson, R. E., Swanson, R. L. and Crowley, H. A.: Perspectives on long-term variations in hypoxic conditions in western Long Island Sound, Journal of Geophysical Research: Oceans, 113, doi:10.1029/2007JC004693, 2008.

Wong, L. A., Chen, J., Xue, H., Dong, L. X., Su, J. L. and Heinke, G.: A model study of the circulation in the Pearl River Estuary (PRE) and its adjacent coastal waters: 1. Simulations and comparison with observations, J Geophys Res-Oceans, 108, 735   doi:10.1029/2002jc001451, 2003.

Xu, C., Xu, Y. J., Hu, J. T., Li, S. Y. and Wang, B.: A numerical analysis of the summertime Pearl River plume from 1999 to 2010: Dispersal patterns and intraseasonal variability, J Marine Syst, 192, 15-27, doi:10.1016/j.jmarsys.2018.12.010, 2019.

740   Yin, K. D., Lin, Z. F. and Ke, Z. Y.: Temporal and spatial distribution of dissolved oxygen in the Pearl River Estuary and adjacent coastal waters, Cont Shelf Res, 24, 1935-1948, doi:10.1016/j.csr.2004.06.017, 2004.

Yu, L., Fennel, K., Laurent, A., Murrell, M. C. and Lehrter, J. C.: Numerical analysis of the primary processes controlling oxygen dynamics on the Louisiana shelf, Biogeosciences, 12, 2063-2076, doi:10.5194/bg-12-2063-2015, 2015.

745

Zhang, H. and Li, S. Y.: Effects of physical and biochemical processes on the dissolved oxygen budget for the Pearl River Estuary during summer, J Marine Syst, 79, 65-88, doi:10.1016/j.jmarsys.2009.07.002, 2010.

Zhang, W., Wu, H., Hetland, R. D. and Zhu, Z.: On Mechanisms Controlling the Seasonal Hypoxia Hot Spots off the 750   Changjiang River Estuary, Journal of Geophysical Research: Oceans, 124, 8683-8700, doi:10.1029/2019jc015322, 2019.

Zhao, H., Tang, D. L. and Wang, D. X.: Phytoplankton blooms near the Pearl River Estuary induced by Typhoon Nuri, J Geophys Res-Oceans, 114, doi:10.1029/2009jc005384, 2009.

755   Zhao, Y., Liu, J., Uthaipan, K., Song, X., Xu, Y., He, B., Liu, H., Gan, J. and Dai, M.: Dynamics of inorganic carbon and pH in a large subtropical continental shelf system: Interaction between eutrophication, hypoxia, and ocean acidification, Limnol Oceanogr, 65, 1359-1379, doi:10.1002/lno.11393, 2020.

Zhou, W., Yin, K., Harrison, P. J. and Lee, J. H. W.: The influence of late summer typhoons and high river discharge on water
760   quality in Hong Kong waters, Estuarine, Coastal and Shelf Science, 111, 35-47, doi:10.1016/j.ecss.2012.06.004, 2012.